Arch. Min. Sci. **63** (2018), 2, 283-300

Electronic version (in color) of this paper is available: http://mining.archives.pl

DOI 10.24425/122448

YANG CAO*, HONGGUANG JI*#, YUEZHENG ZHANG*#, SONG LI**

STUDY ON DISTRIBUTION OF CO AND CONCENTRATION PREDICTION IN BLIND GALLERY AFTER BLASTING OPERATION

BADANIE I PROGNOZOWANIE ROZKŁADU STĘŻENIA CO W ŚLEPYM WYROBISKU PO ZAKOŃCZENIU PRAC STRZAŁOWYCH

It is meaningful to study the issues of CO migration and its concentration distribution in a blind gallery to provide a basis for CO monitoring and calculation of fume-drainage time, which is of a great significance to prevent fume-poisoning accidents and improve efficiency of an excavation cycle. Based on a theoretical analysis of a differential change of CO mass concentration and the CO dispersion model in a fixed site, this paper presents several blasting fume monitoring test experiments, carried out with the test location to the head L_P in arrange of 40-140 m. Studies have been done by arranging multiple sensors in the arch cross-section of the blind gallery, located at the Guilaizhuang Gold Mine, Shandong Province, China. The findings indicate that CO concentrations in the axial directions are quadratic functions with the Y and Z coordinate values of the cross-section of the blind gallery in an ascending stage of CO time--concentration curve, with the maximum CO concentrations in Y = 150 cm and Z = 150 cm. Also, the gradients of CO concentration in the gallery are symmetrical with the Y = 150 cm and Z = 150 cm. In the descending stage of CO time-concentration curve, gradients of CO concentration decrease in lateral sides and increase in the middle, then gradually decrease at last. The rules of CO concentration distribution in the cross-section are that airflow triggers the turbulent change of the CO distribution volume concentration and make the CO volume concentration even gradually in the fixed position of the gallery. Moreover, the CO volume concentrations decrease gradually, as well as volume concentration gradients in the cross-section. The uniformity coefficients of CO concentration with duct airflow velocities of 12.5 m/s, 17.7 m/s and 23.2 m/s reach near 0.9 at 100-140 m from the heading to the monitoring spot. The theoretical model of a one-dimensional migration law of CO basically coincides with the negative exponential decay, which is verified via fitting. The average effective turbulent diffusion coefficient of CO in the blind gallery is approximate to 0.108 m^2/s. There are strong linear relationships between CO initial concentration, CO peak concentrations and mass of explosive agent, which indicates that the CO initial concentration and the CO peak concentration can be predicted, based on the given range of the charging mass. The above findings can provide reliable references to the selection, installation of CO sensors and prediction of the fume-drainage time after blasting.

Keywords: CO concentration distribution; time-concentration curve; uniformity coefficient; dispersion coefficient; attenuation index; fume-drainage time

* SCHOOL OF CIVIL AND RESOURCE ENGINEERING, UNIVERSITY OF SCIENCE AND TECHNOLOGY BEIJING, BEIJING 100083, CHINA

** GUILAIZHUANG MINING CO. LTD., SHANDONG GOLD GROUP, LINYI, 273307, CHINA

\# Corresponding authors: jihongguang@ces.ustb.edu.cn; yuezheng20053660@163.com

Badania migracji, rozpływu i rozkładu stężenia CO w ślepym wyrobisku są niezbędne, stanowią one bowiem podstawę do skutecznego monitorowania poziomu CO i obliczania czasu niezbędnego na usunięcie z wyrobiska szkodliwych gazów – jest to kwestia kluczowa dla zapobiegania wypadkom związanych z zatruciem spalinami oraz dla planowania przebiegu prac wydobywczych. W oparciu o teoretyczną analizę zmian stężenia masowego CO i wykorzystując model dyspersji gazu w stałym punkcie, w pracy przedstawiono wyniki eksperymentów przeprowadzonych w ramach monitorowania stężeń gazów powybuchowych w wyrobisku LP na odległości 40-140 m od czoła wyrobiska. Badania prowadzono przy wykorzystaniu zestawu czujników rozmieszczonych w wybranych punktach ślepego wyrobiska w kopalni złota Guilaizhuang, w prowincji Shandong, Chiny. Wyniki badań wskazują, że stężenia CO w kierunkach poosiowych są funkcjami kwadratowymi wartości współrzędnych Y i Z przekroju przekroju ślepego wyrobiska w zakresie krzywej opadającej na wykresie opisującym zależność stężenia CO od czasu, przy czym maksymalne stężenia CO stwierdzono dla Y =150 cm i Z = 150 cm. Ponadto, wykazano że gradienty stężenia CO w wyrobisku są symetryczne dla Y =150 cm i Z =150 cm. W zakresie krzywej rosnącej na wykresie zależności stężenia CO od czasu gradienty stężenia CO wykazują spadek w końcowych regionach wykresu, w środkowej części wykresu notuje się jego wzrost, po czym znów następuje spadek. Na rozkład stężenia CO w tym przekroju wpływ ma fakt że przepływ powietrza wywołuje turbulentne zmiany stężenia objętościowego CO, następnie stężenie objętościowe maleje systematycznie w dalszych częściach wyrobiska. Ponadto, stwierdzono że stężenie CO a także gradienty stężenia objętościowego w przekroju maleją stopniowo. Współczynniki wyrażające równomierność stężenia CO przy przepływach powietrza z prędkością 12.5 m/s 17.7 m/s i 23.2 m/s osiągają wartość 0.9 w punkcie kontrolnym odległym od wyrobiska o 100-140 m. Teoretyczny model jednowymiarowego rozpływu CO zasadniczo pokrywa się z wzorem zależności wykładniczej z wykładnikiem ujemnym, co zostało potwierdzone w procedurze pasowania. Średnia wartość współczynnika dyfuzji CO dla przepływu turbulentnego w ślepym wyrobisku wyniosła 0.108 m2/s. Stwierdzono istnienie silnej zależności liniowej pomiędzy początkowym stężeniem CO, szczytową wielkością stężenia oraz masą użytego materiału wybuchowego, która wskazuje na możliwość prognozowania początkowego i szczytowego stężenia CO w oparciu o zakres wielkości użytego ładunku wybuchowego. Przedstawione wyniki badań stanowić mogą wiarygodną podstawę dla wyboru rodzaju i miejsca zainstalowania czujników CO oraz do prognozowania czasu wymaganego na usuniecie szkodliwych gazów po zakończeniu prac strzałowych.

Słowa kluczowe: rozkład stężenia CO, zależność stężenia od czasu, współczynnik określający równomierność stężenia, współczynnik dyspersji, współczynnik wyrażający spadek stężenia, czas usuwania szkodliwych gazów po zakończeniu prac strzałowych

1. Introduction

In metal mines, blasting operation is widely used in underground excavation, especially rock drift excavation, due to the advantages of lower cost, simpler operation and stronger applicability. However, during this process, large amount of toxic gases such as CO, NO_x is generated by the detonation, because there are many uncontrollable factors breaking the zone-oxygen balance. This indicates that the oxygen element was consumed during the explosion. The poisonous gases are the root reason for the occurrence of a blasting fume poisoning accident (Cao et al., 2015). In order to avoid occurrence of poisonous accidents, monitoring of CO gas and prediction of fume-drainage time after blasting are very significant daily works in drift excavation, not only for ensuring safety of the miners and their health, but also for instruction of a highly-efficient excavation (Ji et al., 2014; Cao et al., 2017.). Therefore, it is indispensable to select the type and range of a CO sensor, which provides an important reference to monitoring accurate concentration values of CO. Also, it is needed to obtain initial CO concentration value, peak CO concentration and turbulent diffusion coefficient of CO in a blind gallery, to predict the fume-drainage time. Based on these, it is meaningful to carry out research in the field and obtain helpful parameters for mining activities.

The distribution of CO in the cross-section and the uniformity of mixing are very important references to guide monitoring of CO and layout of the CO sensors. There are some theoretical and laboratory research on the movement and composition of the tracing gases, which are more inclined to the residential construction than to underground galleries (Wang et al., 2007; Zhou & Chen, 2013; Chen et al., 2008; Zeng et al., 2011; Li et al., 2013). Simulative research is also conducted on the migration of methane in the galleries (Li, 2013). Also, studies on the propagation law of harmful gases with high-concentration in the galleries were carried out (Lu et al., 2000). At the same time, articles on concentration distribution of CO in blasting fume, uniformity of CO and calculation of peak concentration of CO are not often published. However, such issues mentioned above, in general provide a critical guidance to installation positions of CO sensors and their selection. There are also studies on CO diffusion from the theoretical method modeling (Ye et al., 2015; Peng et al., 2009; Torno et al., 2013) and numerical simulation (Yang et al., 2011; El-Fawal, 2011; Deng et al., 2014), allowing to describe CO migration after blasting and to obtain the empirical formula for the prediction of the exhaust time. However, fewer findings on CO longitudinal dispersion coefficient, attenuation index and initial CO concentration may create great difficulties in calculating and predicting of the fume-drainage time after the explosion or even make it impossible. Therefore, this paper attempts to obtain the relevant parameters via carrying out the monitoring tests of CO in the fume in the gallery, and tries to provide important references for the selection and arrangement of the CO sensors and the prediction of the dilution time after blasting.

2. General law of migration of blasting pollutant

2.1. Unit cube analysis of blasting pollutant

In a forced ventilation, migration of blasting pollutant appertains to a theoretical question of a fluid substance. Let's assume that there is an ideal unit cube with dimensions of *dx*, *dy*, *dz* in the gallery. Also, the following assumptions to this unit cube can be done: air in the unit cube is uncompressed and non-viscous; no CO generation and disappearance in the unit cube because of physical, chemical or biological factors; temperature, pressure, humidity are consistent in the unit cube; CO inlets are on the left, downward, and front sides of the unit cubic and CO outlets are on the right, upward, and back sides of the unit cube. The unit cube is showed in the Fig. 1 below.

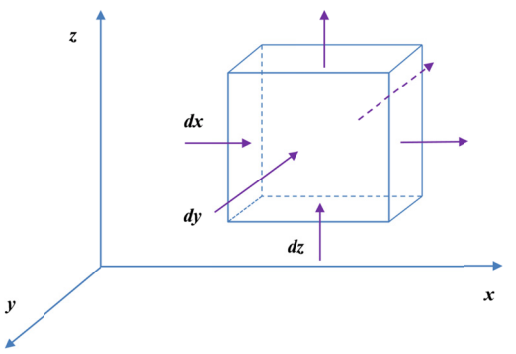

Fig. 1. Schematic diagram of an ideal unit cube of CO dispersion

The migration of CO in the unit cube results from the CO concentration gradient and velocity of the gas. According to the mass conservation and Fick's law, the increment of mass of CO in the unit cube equals to the inlet CO mass minus the outlet CO mass. An equation can be concluded as follows (Chen et al., 2008):

$$\frac{\partial m(x,y,z,t)}{\partial t}+\frac{\partial\left[\overline{u_x}\cdot\partial m(x,y,z,t)\right]}{\partial x}+\frac{\partial\left[\overline{u_y}\cdot\partial m(x,y,z,t)\right]}{\partial y}+\frac{\partial\left[\overline{u_z}\cdot\partial m(x,y,z,t)\right]}{\partial z}$$
$$=E_x\frac{\partial^2 m(x,y,z,t)}{\partial x^2}+E_y\frac{\partial^2 m(x,y,z,t)}{\partial y^2}+E_z\frac{\partial^2 m(x,y,z,t)}{\partial z^2} \tag{1}$$

where:

$m(x,y,z,t)$ — means mass concentration function of CO, mg/m^3;

$\overline{u_x}$, $\overline{u_y}$, $\overline{u_z}$ — mean average velocities, respectively in a direction of x, y and z axis, m/s;

E_x, E_y, E_z — stand for the average values of turbulent coefficient in a direction of x, y and z axis, m/s^2;

If only turbulent dispersion in a direction of x axis is taken into consideration, further assumption of $\overline{u_y}=\overline{u_z}=0$ can be inserted to the Eq. (1). In this case, the Eq. (1) could be simplified to the form as below:

$$\frac{\partial m(x,t)}{\partial t}+\frac{\partial\left[\overline{u_x}\cdot m(x,t)\right]}{\partial x}=E_x\frac{\partial^2 m(x,t)}{\partial x^2} \tag{2}$$

Boundary conditions of CO mass concentration function of the unit cube can be obtained as follows:

$$\begin{cases}\int_0^l\int_0^{+\infty} m(x,t)\ dxdt=M\\ m(0,0)=m(L_0,0)=m_0\\ M=m_0\cdot S\cdot L_0\\ \lim\limits_{\substack{t\to\infty\\ x\to\infty}} m(x,t)=0\end{cases} \tag{3}$$

$m(x,t)$ — means the mass concentration function of CO in the unit cube;

M — represents total mass of CO generated after blasting, g;

m_0 — stands for the initial mass concentration of CO in the control volume, mg/m^3;

S — means the cross-section of a gallery, m^2;

$\boldsymbol{L_0}$ — is the cast length of a blasting fume, m;

l — means the length of a blind gallery, m.

Therefore, the migration of CO in a blasting fume could be transferred into the solution of a partial differential equation. The mass concentration function $m(x,t)$ can be deduced from Eq. (2) as below (Li, 1989):

$$m(x,t)=\frac{m_0 L_0}{2\sqrt{\pi E_x t}}\exp\left\{-\frac{\left(x-\overline{u_x}t\right)^2}{4E_x t}\right\} \tag{4}$$

where:

x — means coordinate value in X-axis, m;
$\overline{u_x}$ — is the average velocity of air in unit cubic, m/s;
m_0 — stands for the average mass concentration of CO in the cross-section, mg/m^3;
t — means the dilution time after blasting, s.

3. Blasting fume monitoring test

Guilaizhuang Gold Mine is located in Shangdong Province, China. This gold mine has begun to oparate more than 40 years ago. In the beginning, the exploitation method was open-pit mining, and then, it was changed to the underground mining method, because of a limit of the pit bottom, which can be seen in the Fig. 2.

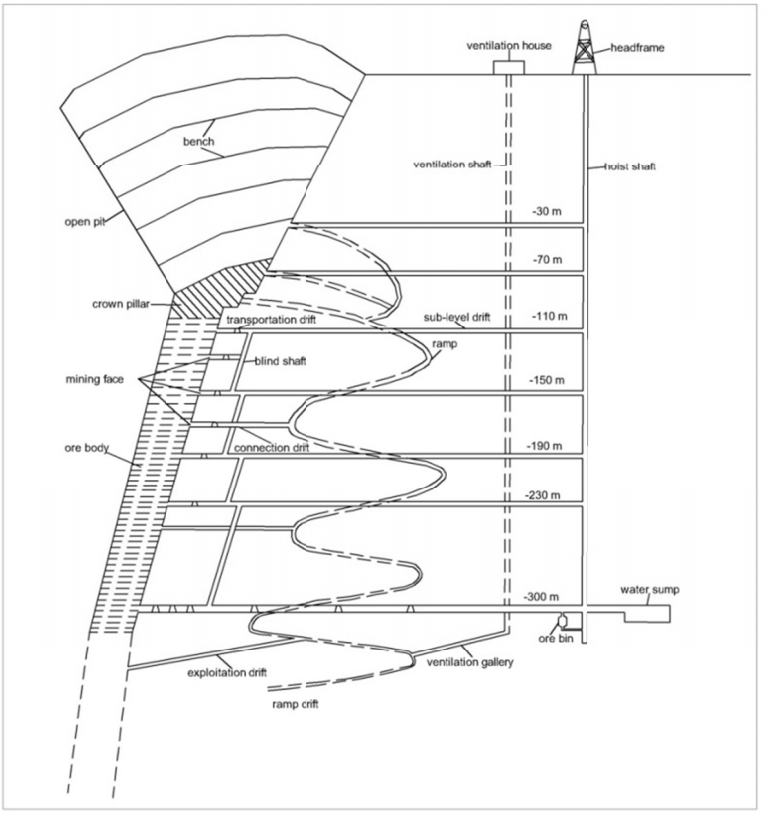

Fig. 2. Profile map of Guilaizhuang Gold Mine in Shangdong Province, China

A series of blasting fume monitoring tests were carried out in a blind gallery, which is located at the level of 110 m. The cross-section shape of the blind gallery is semi-circular arch with a width of 3.0 m and a height of 3.0 m. Explosive agent used for excavation is the No. 2 rock emulsion with charging mass ranging from 16 kg to 40 kg. The pattern of auxiliary ventilation is forcing ventilation. The diameter of a duct is 40 cm. The distance from the duct outlet to the heading is about 12 m to 24 m. It can be assumed that there is no leakage of the duct. Carbon monoxide is selected as the monitored gas, which could represent migration of the blasting fume because of stable chemical and physical properties and a relatively high concentration, easy to be measured. Carbon monoxide wireless sensors (specification in Tab. 1 below) were installed to obtain CO concentration values in the cross-section at the coordinates of Y = 50 cm, 100 cm, 150 cm, 200 cm and 250 cm, as well as Z = 50 cm, 100 cm, 150 cm, 200 cm and 250 cm. The sensors record and upload the values every 20 s. Monitoring tests were carried out more than ten times in the blind gallery in different dates, but only eight recorded sets of data (Tab. 2) could be eligible for further processing. For each monitoring test, the duration was about 2-3 hours. Localization of the sensors was chosen to monitor the alteration of CO concentration in the cross-section of the gallery. The layout of the monitoring test in the blind gallery and sensors distribution are shown in Fig. 3.

TABLE 1

Specification of CO sensor

Name	Output Frequency	Technical Parameters
GHT500 CO Sensor	433MHZ	Measurement range: 0-2000 ppm; Measuring error: 0-100 ppm, no more than ±(1.5+2.0%) > 100-500 ppm, no more than ±4.0% Wireless connection External power supply or internal battery; Working voltage: 10.5-14.5V.

TABLE 2

Data of CO monitoring tests

Date	Level / m	Cross-section area/ m^2	Explosive mass/ kg	L_P /m	L_0 /m	Duct velocity m/s
29 Aug, 2014	#28 –110 m	8.04	32	40	20	16.5
30 Aug, 2014	#28 –110 m	8.04	40	60	12	17.1
2 Sep, 2014	#28 –110 m	8.31	24	80	14	18.1
4 Sep, 2014	#28 –110 m	8.84	24	100	18	15.3
6 Sep, 2014	#28 –110 m	8.31	36	120	17	16.7
9 Sep, 2014	#28 –110 m	8.31	16	140	20	17.3
10 Sep, 2014	#28 –110 m	8.31	28	140	19	15.6
13 Sep, 2014	#28 –110 m	8.31	24	140	24	15.9

3.1. Distribution of CO concentration in the axes

Dilution time after blasting mainly refers to the time, after which CO or other poisonous gases concentration in the blasting fume declines to the safety exposure limits of the regulations or laws, generally regarding value of the CO concentration lower than the exposure limit as the

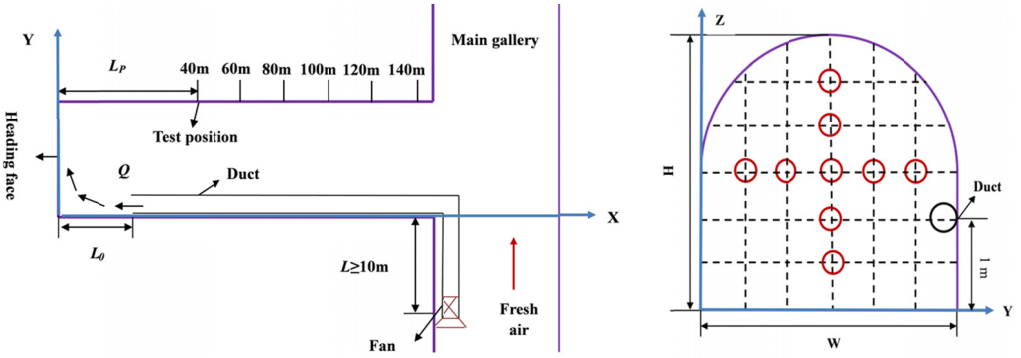

Fig. 3. Schematic map of the blind gallery and sensors in the cross section.
Please notice X, Y and Z axes marked in the graphs

reference. Through conducting the CO monitoring tests, it is can be found that: fume-drainage time in the CO concentration-time curve is generally divided into concentration-ascending duration and concentration-descending duration. The CO ascending duration refers to the time interval from completion of the blasting operation to the appearance of the CO peak concentration in the monitoring location, which lasts in a range from several to more than ten minutes. The CO descending duration starts from the CO peak concentration time to the safe exposure limit of CO, which typically lasts for a few hours, accounting for the main part of the dilution time after blasting. Four sets of data taken from the blasting fume monitoring tests include two groups of Y axis and two group of Z axis. Each set of data derives from the CO concentration-time curve, including one time point from the CO ascending curve and two time points from the CO descending curve. In the Y-axis direction of the gallery, it is noted that CO concentrations at the three time points firstly increase, and then decrease with the Y-axis coordinate value, and the maximum CO concentration is located at the Y = 150 cm. The fitting curves between the CO concentration and the Y coordinate values of the four groups of the ascending segments show that the two pairs of data are quadratic, and the parabolic symmetry axis is basically at the Y = 150 cm. In the ascending part of the curve, the CO concentration gradients in Y-axis are more evenly and symmetrically distributed. Afterwards, CO concentration gradients in the descending section change. First, the CO concentration gradients on both sides of the Y-axis decrease, and the CO concentration gradients in middle part increase. Then, the concentration gradient of CO on both sides and middle side of the Y-axis decrease, and the CO concentration gradient on two sides tend to be 0. Meanwhile, the CO concentration gradients in the CO descending section are also symmetrical. The changes of CO concentrations are mainly due to the turbulence deformation under the action of airflow, and the changes of concentration gradients are mainly due to the combined action of molecular motion, temperature, density unevenness and turbulence pulsation. The changes of CO concentration in the gallery in the Y axis are shown in Fig. 4 below.

The obtained results show that the CO concentration at the three time points increases firstly, and then decreases with the Z-axis coordinate value, and the maximum CO concentration is at Z = 150 cm in the gallery. The fitting curves between the CO concentration and the Z coordinate values of the two groups are found to be quadratic, and the parabolic symmetry axis is basically at Z = 150 cm. However, the CO concentration gradients in the CO descending section change

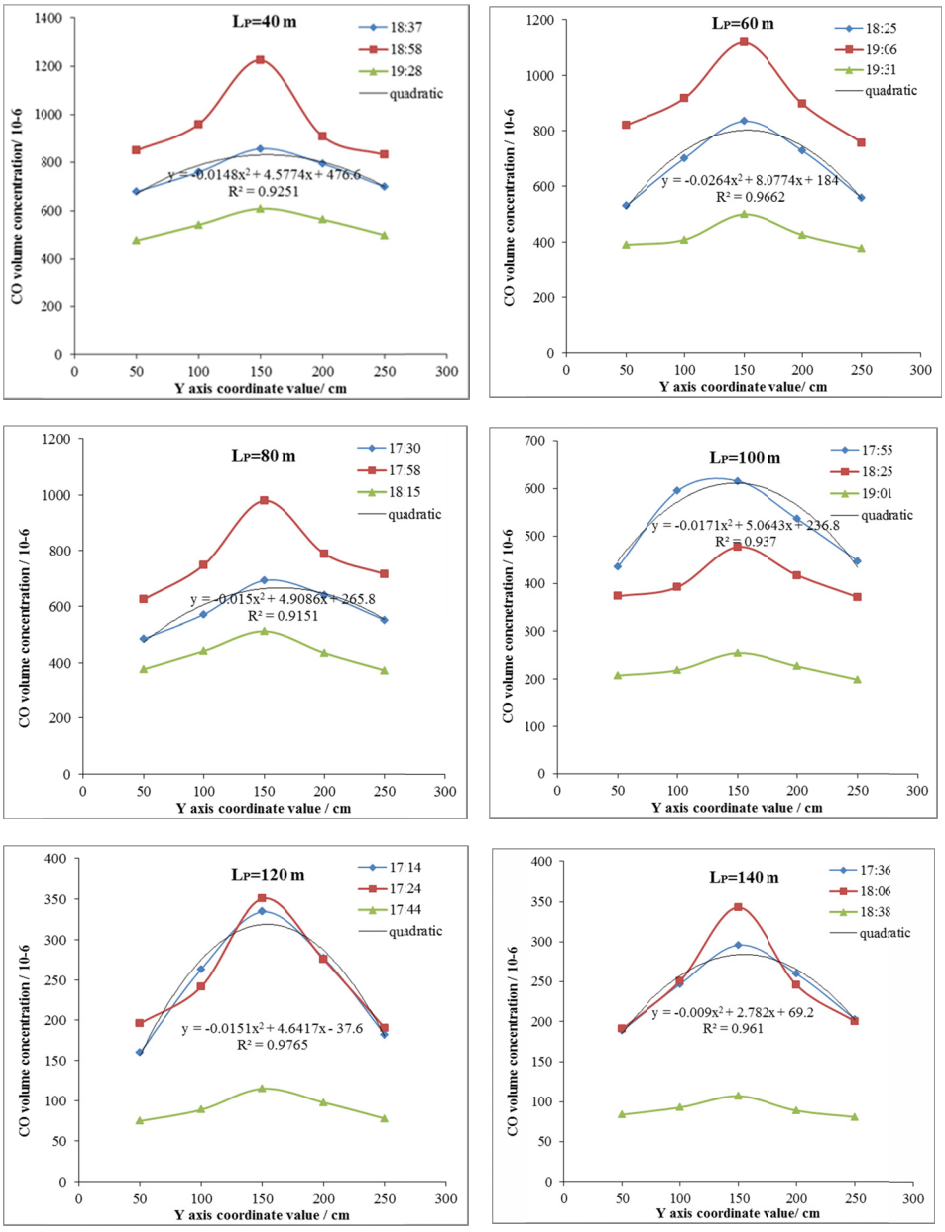

Fig. 4. CO concentrations in the Y-axis in cross-section of the blind gallery

later. The CO concentration gradients on both sides of the gallery in the Z-axis decreases first, while the gradients of CO in the middle part increase. Then, the gradients of CO concentration in the whole cross-section of the gallery decrease. Meanwhile, in the CO descending section, the CO concentration gradients also have symmetrical distributions, however, their trend fluctuates

slightly. Such fluctuation is, on the one hand, likely coming from a fact that in the number of the monitoring groups there are random errors in the measurements, but on the other hand, may be caused by instable airflow in the Z-axis direction. The gradient of CO concentration on the roadway in the Z-axis is shown in Fig. 5.

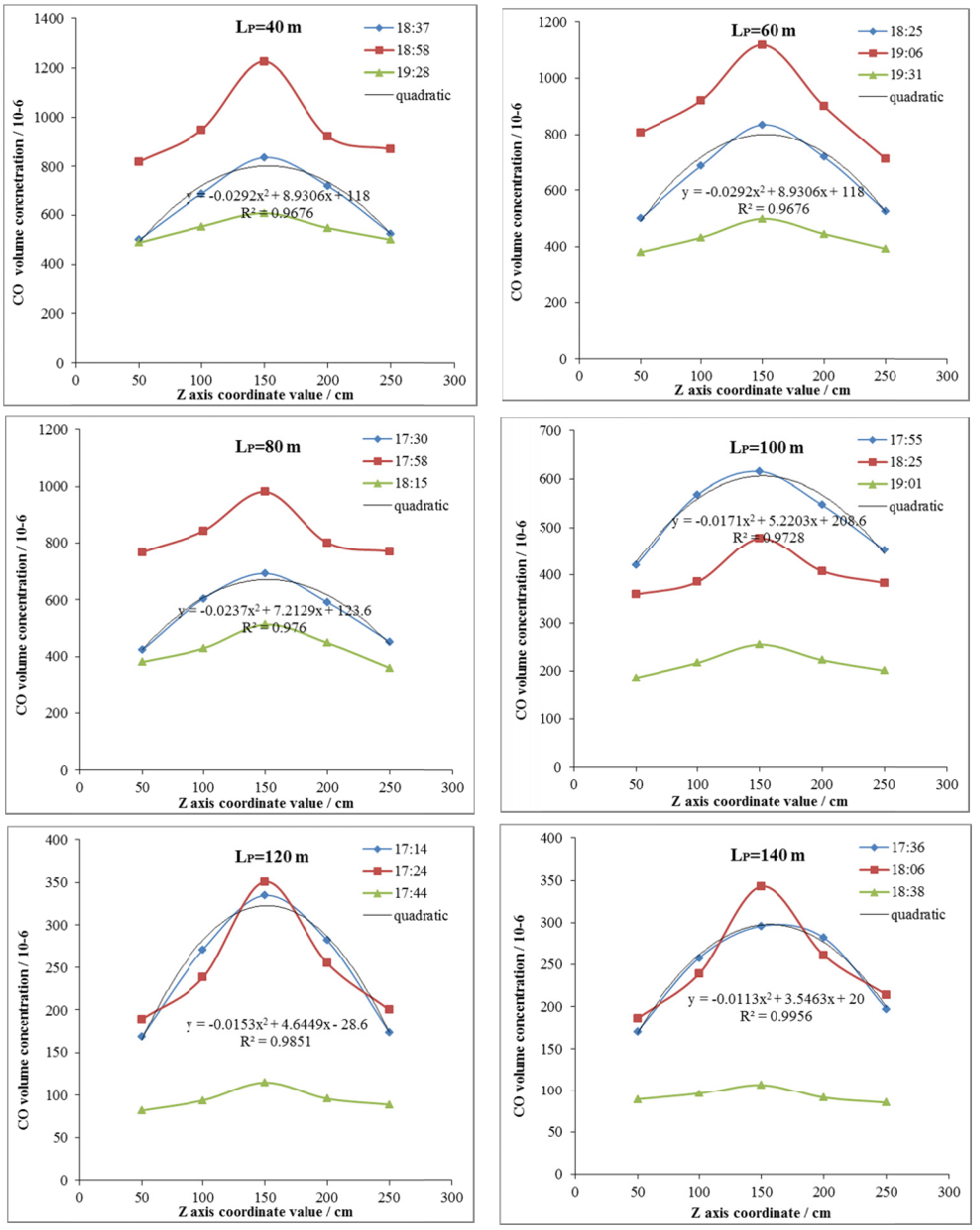

Fig. 5. CO concentrations in the Z-axis in cross-section of the blind gallery

3.2. CO concentration distribution in the cross-section

As an example, the CO concentration distributions in cross-section of the blind gallery with three time points when $\mathbf{L_P}$ = 40 m are illustrated in Fig. 6. It can be observed that the CO concentration in the cross-section present different distribution laws in these three time points. At the time point of 18:37, the CO is evenly contributed in the gallery in the ascending stage of CO volume concentration-time curve. The contour lines of CO concentration are very close to each other, which indicate that the CO volume gradients are very high. At time point of 18:58, the CO volume concentrations rise in the peak of CO volume concentration-time curve, because of uneven distribution of the CO volume concentration when the duct supplies continuous airflow to the heading. In this stage, the CO volume concentration is much higher in the middle of the cross-section than at the two sides. This indicates that the airflow triggers the turbulent change of the CO distribution volume. On one hand, the airflow which makes a change of a shape of the

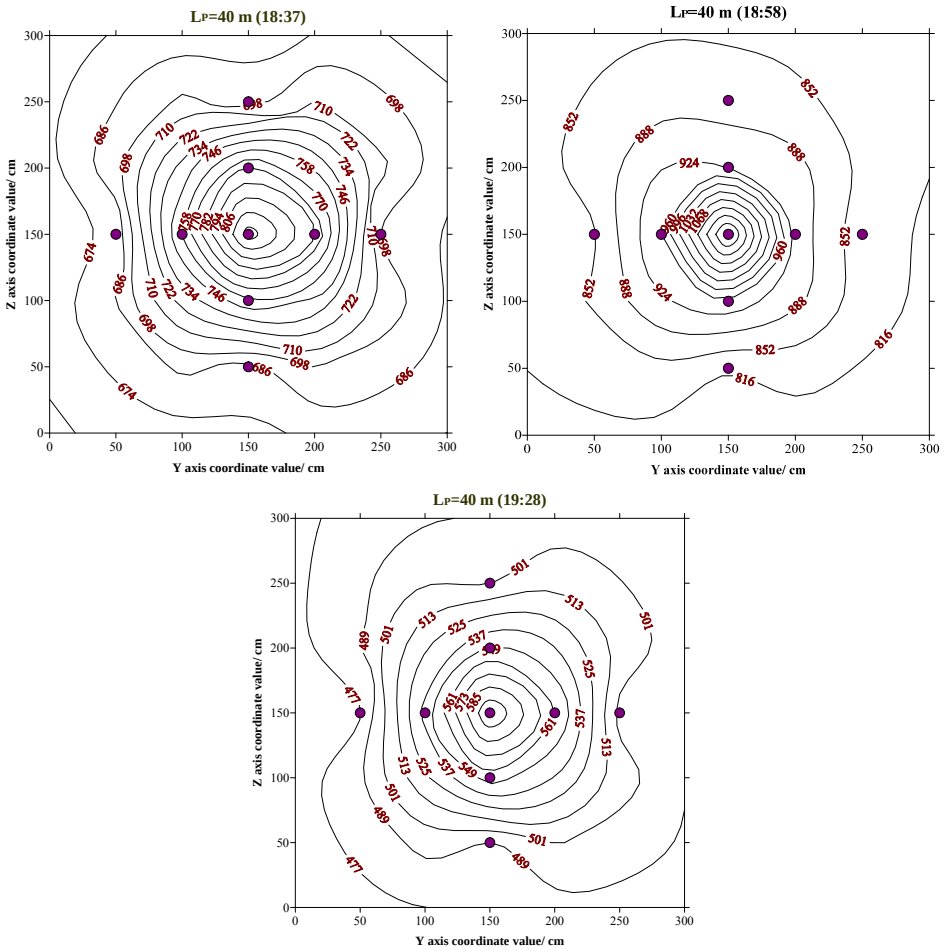

Fig. 6. CO concentration distribution in the cross-section with L_P = 40 m

blasting volume results in the uneven distribution of CO volume concentration, but on the other hand, the airflow velocity gradient brings about the high-concentration of CO accumulated in the middle of the cross-section and migrated towards the entrance of the gallery. At 19:28, the time point selected from the descending stage of the CO volume-concentration curve, the CO volume concentration is much lower than at the peak stage and is gradually distributed more evenly. The CO volume concentration gradients decrease because of the diffusion of CO in the gallery and dispersion of CO to the main gallery.

As an example, CO volume concentration distributions, in the peak stage of the CO volume concentration-time curve, in a different cross-section of the gallery with different $\mathbf{L_P}$ values are presented in the Fig. 7 below. With the increase of $\mathbf{L_P}$ values from 40 m to 120 m, the CO volume concentrations decrease gradually. CO volume concentration gradients in the cross-section decrease. The CO concentration gradients at $\mathbf{L_P}$ = 40, 60 m are not evenly distributed in the cross-section, but become gradually distributed more evenly with an increase of $\mathbf{L_P}$ values.

3.3. CO uniformity in the cross-section

During the process of longitudinal turbulent dispersion of CO in the blind gallery, the distance, at which CO is evenly mixed in the whole cross-section, is very important for obtaining accurate measurements of CO concentrations. According to the Eq. [5], the uniformity coefficient is the ratio of the side concentration (minimum) to the central concentration (maximum) in the gallery. When the general uniformity coefficient is 0.9 or more, it is considered that the CO in whole cross section is in fact uniformly mixed. The CO uniformity coefficient is expressed as:

$$c = \frac{C_{\min}}{C_{\max}} \tag{5}$$

First of all, some assumptions should be given as follows: 1) there are no air leakages in the forcing duct-line; 2) the mean velocity in each of the measured cross-sections was constant. In the tests, five monitoring locations were selected and CO sensors were installed in the side positions (Y = 50 cm, 250 cm) and the middle positions (Y = 150 cm) which are at 60 m, 80 m, 100 m, 120 m and 140 m in the gallery. Also, a varying duct airflow speed of 12.5 m/s, 17.7 m/s and 23.2 m/s, was tested, respectively. Obviously, different duct airflow has different ability to dilute the pollutants in the gallery. After calculating CO uniformity coefficients of the cross-section in each monitoring points, the relationship between the uniformity coefficients and the distance from the monitoring point to the heading could be obtained in the Table 3, which is graphed as shown in Fig. 8 below. It can be found that for each set of data of the three speeds, the CO uniformity coefficients increase with the longer distance from the monitoring point to the heading. The CO uniformity coefficients are on the order of 0.9 or more when the distance from the measuring point to the heading reaches 100-140 m. It can be seen that the CO in the cross-section has been mixed evenly at the distance of about 100-140 m from the head and can be regarded as the CO concentration level at any point of the cross-section. In particular, when the duct airflow velocity is 12.5 m/s, 17.7 m/s and 23.2 m/s, the distance of the CO uniformity coefficient reaching 0.9 are approximately 140 m, 120 m and 100 m, respectively. It can be indicated that with the larger velocity of the airflow in the duct provided, the shorter is the distance for even distribution of CO in the cross-section. Therefore, faster airflow velocity can contribute more to the acceleration of CO uniformity in the gallery.

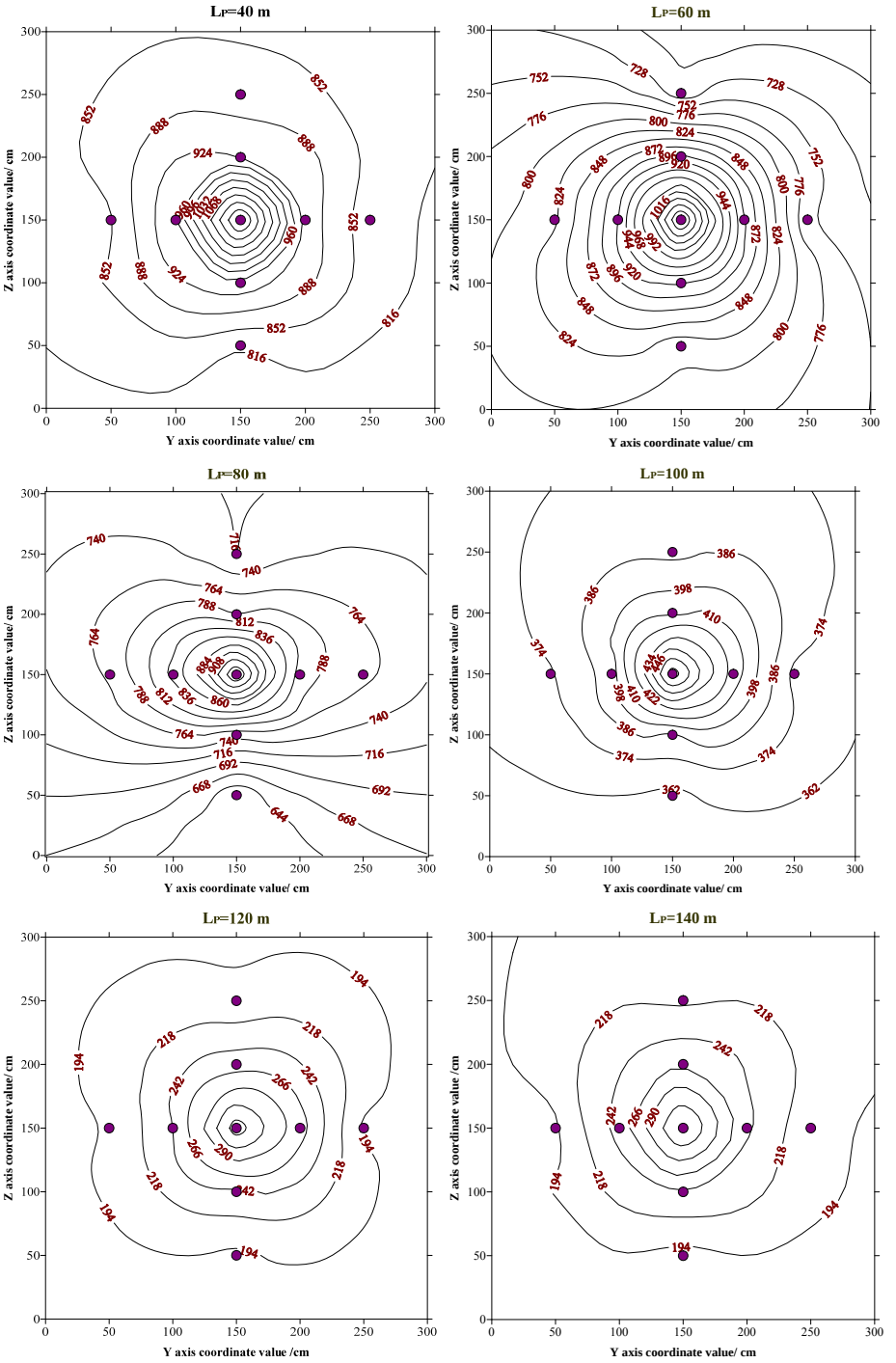

Fig. 7. CO volume concentration distribution in the cross-section with different $\mathbf{L_P}$ values

TABLE 3

CO uniformity coefficients in different $\mathbf{L_P}$ values with different duct velocities

Duct velocity / m · s^{-1}	L_P / m				
	60	80	100	120	140
13.3	0.733	0.751	0.862	0.882	0.906
17.7	0.802	0.854	0.869	0.898	0.907
23.2	0.831	0.865	0.899	0.912	0.909

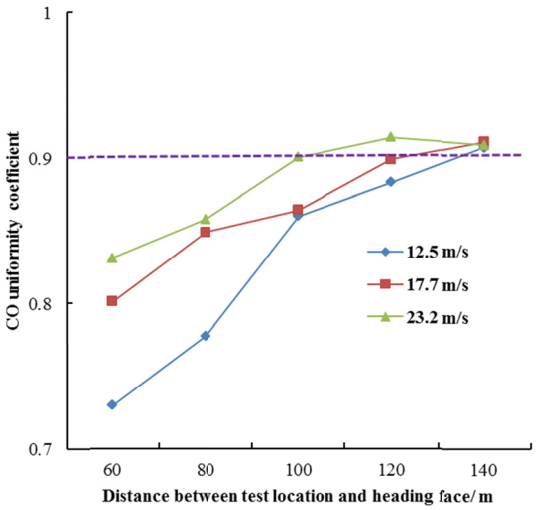

Fig. 8. Relationship between test distance and CO uniformity coefficient in the cross section with various duct speeds

4. Diffusive parameters of blasting fume

4.1. Effective turbulent diffusion coefficient

The following discussion and equations are about concentration of CO in the "*E* distribution" presented in Fig. 9. The considered axis of symmetry is $x = v \cdot t_m$. When assuming $x = x_0$ ($x_0 > 0$) and drawing a parallel line to the *t*-axis, two intersections can be obtained with the $m(x, t) - t$ curve, as shown in the Fig. 9.

For CO concentration values $m(x, t_1)$ and $m(x, t_2)$ in the $C(x, t) - t$ curve, a series of equations can be obtained as follows:

$$m(x,t_1) = m(x,t_2) \tag{6}$$

$$m(x,t_1) = \frac{m_0 L_0}{2\sqrt{\pi E_x t_1}} \exp\left\{-\frac{\left(x-\overline{u_x}t_1\right)^2}{4E_x t_1}\right\} \tag{7}$$

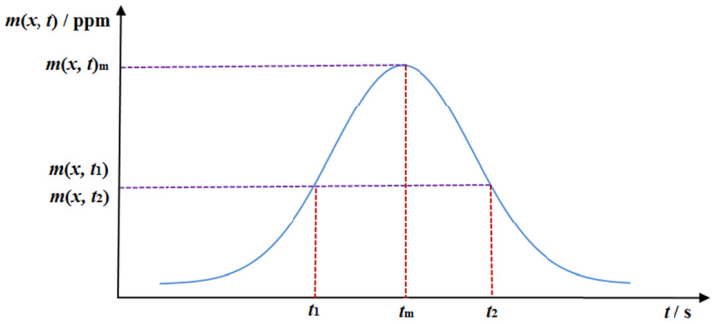

Fig. 9. CO concentration-time curve in a given location in the gallery

$$m\left(x,t_2\right)=\frac{m_0L_0}{2\sqrt{\pi E_x t_2}}\exp\left\{-\frac{\left(x-\overline{u_x}t_2\right)^2}{4E_x t_2}\right\} \tag{8}$$

After using natural logarithm on double sides of the Eq. (7) and the Eq. (8), the following forms can be written:

$$\ln m\left(x,t_1\right)=\ln\frac{m_0L_0}{2\sqrt{\pi E_x t_1}}-\frac{\left(x-\overline{u_x}t_1\right)^2}{4E_x t_1} \tag{9}$$

$$\ln m\left(x,t_2\right)=\ln\frac{m_0L_0}{2\sqrt{\pi E_x t_2}}-\frac{\left(x-\overline{u_x}t_2\right)^2}{4E_x t_2} \tag{10}$$

In a further step, the Eq. (11) can be formulated as a result of subtraction between Eq. (9) and Eq. (10):

$$\ln\frac{m_0L_0}{2\sqrt{\pi E_x t_1}}-\ln\frac{m_0L_0}{2\sqrt{\pi E_x t_2}}=\frac{\left(x-\overline{u_x}t_1\right)^2}{4E_x t_1}-\frac{\left(x-\overline{u_x}t_2\right)^2}{4E_x t_2} \tag{11}$$

$$\ln\sqrt{\frac{t_2}{t_1}}=\frac{\left(t_2-t_1\right)\left[x^2-\overline{u_x}^2t_1t_2\right]}{4E_x t_1t_2} \tag{12}$$

Eq. (13) and Eq. (14) can be obtained from the Fig. 9 according to the property of the "*E* distribution" curve:

$$t_{\mathrm{m}}=\frac{t_1+t_2}{2} \tag{13}$$

$$t_m=\frac{x}{u_x} \tag{14}$$

If replacing x in the Eq. (12) and according to the Eq. (13) and Eq. (14), a new form of Eq. (12) can be written as:

$$\ln\sqrt{\frac{t_2}{t_1}} = \frac{(t_2 - t_1)\left[\overline{u_x}^2\left(\frac{t_1 + t_2}{2}\right)^2 - \overline{u_x}^2 t_1 t_2\right]}{4E_x t_1 t_2} \tag{15}$$

$$E_x = \frac{\overline{u_x}^2 (t_2 - t_1)^3}{8t_1 t_2 \ln(t_1 / t_2)} \tag{16}$$

According to the Eq. (16), effective turbulent coefficient E_x can be calculated the based on the eight CO concentration-time curves from the blasting monitoring tests, as demonstrated in the Table 4.

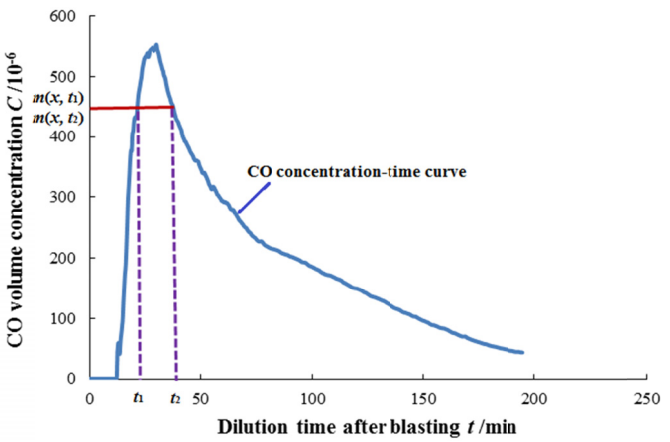

Fig. 10. Calculation of the effective turbulent diffusion coefficient

TABLE 4

Effective turbulent diffusion coefficients of CO

Parameter / No	t_1 s	t_2 s	u_x m/s	E_x m/s^2
1	540	1560	0.031	0.143
2	560	1200	0.038	0.092
3	720	1440	0.041	0.109
4	120	360	0.051	0.095
5	540	1380	0.033	0.116
6	360	1200	0.029	0.119
7	204	624	0.040	0.104
8	960	1560	0.049	0.089
CO mean turbulent diffusion coefficient E_x				0.108

4.2. Prediction of CO concentration

Dilution time after blasting operation is an important factor for heading cycle. According to the Eq. (4), the initial CO concentration in the cast area is a critical element for calculation of the dilution time and is directly decided by a mass of the explosive agent. Theoretically, generation of the CO mass is linearly proportional to the mass of the explosive, with a theoretical multiplier present. However, the actual effective multiplier is generally decided by the charging pattern, temperature, moisture, rock property, etc. Based on results from the fume monitoring tests, 8 sets of data were collected with the initial concentration of CO and the explosive agent mass (Tab. 5), and were fitted with a liner relationship between the initial concentration of CO and the explosive agent mass, as presented in the Fig. 11. The fitted Eq. (17) can be obtained as follow:

$$C_0 = 27.345\ \mathrm{m} - 47.078 \tag{17}$$

where C_0 — means the initial concentration of CO in the blasting cast area, ppm; m — stands for the mass of the explosive agent, kg.

TABLE 5

CO concentration values and the corresponding mass of the explosive agent

No.	CO fitting value C_0 / ppm	CO peak value CO_{max} / ppm	Mass of explosive agent m / kg
1	803.2	527.3	32
2	970.3	696.5	40
3	654.4	437.8	24
4	552.2	430.9	24
5	1011.1	707.8	36
6	364.7	219.8	16
7	801.1	535.6	28
8	591.7	319.1	24

From the Fig. 11 it can be found that there is a strong linear relationship between the CO initial concentration and the mass of the explosive with a fitting degree $R^2 = 0.9257$. For the given mass of charging, the CO initial concentration can be predicted when mass of the explosive agent is in a range from 16 to 40 kg.

Besides, accurate measurements of CO concentration make good preparation for the further calculations. The peak concentration of CO in the gallery can provide reference to selecting the CO sensor, especially its range and accuracy. Also, in the range of 16 to 40 kg of the charging mass, the fitting curve between the CO peak concentrations and the charging mass of the explosive agent can be obtained, as shown in Fig. 11 and Eq. (18) is shown as below:

$$C_0 = 21.012\ m - 103.97 \tag{18}$$

where: C_{max} — means the CO peak concentration, ppm; m — stands for the mass of the explosive agent, kg.

The findings reveal that there is a good linear relationship between the CO peak concentration and the mass of the charging explosive agent with a fitting degree $R^2 = 0.9104$. This can offer a favorable support to predict the peak concentration in the gallery and reliable accordance to selection of CO sensors for monitoring.

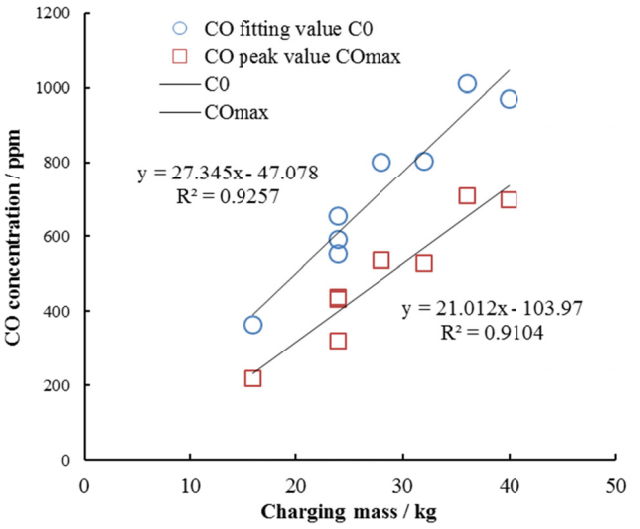

Fig. 11. Fitting curves between CO concentrations and the charging mass

5. Conclusions

(1) This paper presents the significance of migration law and parameters regarding CO gas in the gallery after blasting operation. Theoretical deduction is presented in the paper and demonstrates the CO concentration law via analyzing the movement of CO in the unit cube.

(2) Through performing the blasting fume monitoring tests, it can be conclude that CO concentrations increase first and then decrease on the Y-axis and Z-axis in the cross-section of the gallery and the maximum CO concentration are at the coordinates of Y = 150 cm and Z = 150 cm. Fitting results show that CO concentrations have a quadratic function relationship with the Y and Z coordinate values and the symmetry axes are approximately at the Y = 150 cm and Z = 150 cm. The CO concentration gradients of the Y and Z axes in the CO concentration ascending stage are more evenly symmetrically distributed. The CO concentration gradients in the roadway first decrease on sides and become larger in the middle, and then decrease in both sides and in the middle of the cross-section. The CO concentration distribution law in the cross-section is as follows: airflow triggers the turbulent change of the CO distribution volume concentration and makes the CO volume concentration gradually even in the fixed position of the gallery; the CO volume concentrations decrease gradually, as well as volume concentration gradients in the cross-section. The CO concentration gradients tend to be zero. Generally, the CO uniformity coefficient in the gallery increases with the increasing distance from the heading to the monitoring location. In particular, when the duct airflow velocity is 12.5 m/s, 17.7 m/s and 23.2 m/s, the distances of the CO uniformity coefficient reaching near 0.9 are approximately 140 m, 120 m and 100 m, respectively in the gallery.

(3) The theoretical equation for the effective turbulent diffusion coefficient is achieved via mathematical deduction. The CO effective turbulent diffusion coefficient in the blind gallery is calculated via illustration of the CO concentration-time curve and obtains a mean value of 0.108 m/s^2, which can offer good reference to prediction of the dilution time after blasting. It

is also found that the amount of the charging mass has a close linear relationship with the CO initial concentration and the CO peak concentration, which can provide reference for CO sensor selection and prediction of the fume-drainage time after blasting operation.

Acknowledgements

The research was funded by the project "The State Key Research Development Program of China (Grant No. 2016YFC0600801)". The authors would like to thank Guilaizhuang Mining Co. Ltd and its personnel for their help in providing valuable data for the study.

References

Cao Y., Ji H.G., You S., Zhou Q.M., 2015. *Research on mechanism of blasting fume poisoning and prevention technology*. Industrial Safety and Environmental Protection **6**, 73-75.

Chen K.Y., Li S.G., Zhang Z.H., 2008. *Theoretic research related to the method of measuring air quantity by means of a tracing gas*. Journal of China University of Mining & Technology **37**, 1, 10-14.

Deng X.H., Liu Z., Liu Z.C., 2014. *3D numerical simulation on forced construction ventilation of long single head tunnel of lianghekou*. Journal of Civil, Architecture & Environmental Engineering **36**, 2, 35-41.

Chen K.Y., Li S.G., Zhang Z.H., He J.J. et al., 2008. *Theoretic research related to the method of measuring air quantity by means of a tracing gas*. Journal of China Univer sity of Mining & Technology **37**, 1, 10-14.

El-Fawal M.M., 2011. *Mathematical modeling for radon prediction and ventilation air cleaning system requirements in underground mines*. Journal of American Science **7**, 2, 389-402.

Ji H.G., Cao Y., Zhang G., 2014. *Prediction of drain-fume time of single-end roadway in tunneling process*. Metal Mine **43**,142-145.

Cao Y., Ji H. Zhou Q., 2017. *Calculation of fume-drainage time of tunnel after blasting*. Journal of Harbin Institute of Technology **49**, 8, 135-140.

Li E.L., 1989. *The longitudinal dispersion model and longitudinal dispersion coefficient of turbulent mass transfer in mine tunnel*. Journal of Fuxing Mining Institution **8**, 3, 65-69.

Li Y.C., Yang S.Q., Zhang S., 2013. *The qualitative identification of air leakage channels in goaf based on the tracer gases*. Safety in Coal Mine **44**, 1, 185-188.

Li Z.X., Wang T.M., Jia J.Z., 2013. *Numerical simulation of migration and diffusion of exogenous gas in mine roadway*. Journal of China University of Mining & Technology **5**, 731-735.

Lu G.L., Li C.S., 2000. *Study on the law of concentrative harmful gas spreading in ventilation network*. Journal of Shandong University of Science and Technology (Natural Sceince) **19**, 2, 120-122.

Peng H., Lei J.S., Yao J.J., 2009. *Research on blasting fume natural diffusion model during tunnel construction*. Subgrade Engineering **6**, 30-31.

Torno S., Toraño J., Ulecia M., Allende C., 2013. *Conventional and numerical models of blasting gas behaviour in auxiliary ventilation of mining headings*. Tunnelling and Underground Space Technology **34**, 73-81.

Yang Z.C., Yang P., Lv W.S., 2011. *Numerical simulation on diffusion law of blasting fume during roadway tunnel across a vein in an alpine mine*. Journal of University of Science and Technology Beijing **33**, 5, 521-525.

Ye Y.J., Jiang J.T., Ding D.X., 2015. *Transport of radon and blasting-fume in blind roadway with exhaust ventilation after blasting*. China Safety Science Journal **25**, 5, 131-137.

Wang L.X., Bai Y.H., Liu Z.R., 2007. *Study on calculation method for measuring air ventilation rate with trace gas of CO_2*. Building Science **23**, 8, 36-40.

Zeng X.Y, Chi Z.H., Zheng M.G., 2011. *Experimental study on the mixing uniformity of tracer gas*. Journal of China University of Metrology **2**, 132-137.

Zhou Y.X., Chen H., 2013. *A review of natural ventilation measurements using tracer gas techniques*. Building Energy & Environment **1**, 54-56.